



Investigating the effects of soil moisture on thermal infrared land surface temperature and emissivity using satellite retrievals and laboratory measurements[☆]

Glynn C. Hulley^{*}, Simon J. Hook, Alice M. Baldridge

Jet Propulsion Laboratory, California Institute of Technology, 4800 Oak Grove Drive, Pasadena, CA, 91109, USA

ARTICLE INFO

Article history:

Received 10 September 2009

Received in revised form 1 February 2010

Accepted 6 February 2010

Keywords:

Thermal infrared

Emissivity

Soil moisture

AIRS

MODIS

ASTER

ABSTRACT

This study investigates the effects of soil moisture (SM) on thermal infrared (TIR) land surface emissivity (LSE) using field- and satellite-measurements. Laboratory measurements were used to simulate the effects of rainfall and subsequent surface evaporation on the LSE for two different sand types. The results showed that the LSE returned to the dry equilibrium state within an hour after initial wetting, and during the drying process the SM changes were uncorrelated with changes in LSE. Satellite retrievals of LSE from the Atmospheric Infrared Sounder (AIRS) and Moderate Resolution Imaging Spectroradiometer (MODIS) were examined for an anomalous rainfall event over the Namib Desert in Namibia during April, 2006. The results showed that increases in Advanced Microwave Scanning Radiometer (AMSR-E) derived soil moisture and Tropical Rainfall Measuring Mission (TRMM) rainfall estimates corresponded closely with LSE increases of between 0.08–0.3 at 8.6 μm and up to 0.03 at 11 μm for MODIS v4 and AIRS products. This dependence was lost in the more recent MODIS v5 product which artificially removed the correlation due to a stronger coupling with the split-window algorithm, and is lost in any algorithms that force the LSE to a pre-determined constant as in split-window type algorithms like those planned for use with the NPOESS Visible Infrared Imager Radiometer Suite (VIIRS). Good agreement was found between MODIS land surface temperatures (LSTs) derived from the Temperature Emissivity Separation (TES) and day/night v4 algorithm (MOD11B1 v4), while the split-window dependent products (MOD11B1 v5 and MOD11A1) had cooler mean temperatures on the order of 1–2 K over the Namib Desert for the month of April 2006.

© 2010 Published by Elsevier Inc.

1. Introduction

Land surface temperature and emissivity (LST&E) products are generated by a host of different sensors with varying spatial, spectral and temporal resolutions. Examples are the Atmospheric Infrared Sounder (AIRS) on NASA's Aqua satellite, the Moderate Resolution Imaging Spectroradiometer (MODIS) on NASA's Terra and Aqua satellite, the Spinning Enhanced Visible and Infrared Imager (SEVIRI) on the METEOSTAT Second Generation-1 (MSG), and the Advanced Spaceborne Thermal Emission and Reflection Radiometer (ASTER) on Terra.

Since all these sensors use different retrieval methodologies for generating LST&E products, it is important to assess their ability to dynamically retrieve variations in LSE due to changes in surface soil moisture (SM), vegetation cover and type, snow/ice dynamics, and surface roughness. In this study we focus on the effects of SM on LSE which can occur due to rainfall events, dew, or from snow melt for example.

Previous studies on the LSE and SM dependence in the TIR are limited, and have involved using laboratory and remote sensing measurements to estimate the LSE and SM relationship for a variety of different types of soils. Mira et al. (2007) showed that emissivity of a variety of different soils varies from 1.7% to 16% with increasing SM content in the quartz reststrahlen band between 8.2 and 9.2 μm , and Salisbury and Daria (1992) found that an increase in SM of 7% resulted in an emissivity increase of 5%. Ogawa et al. (2006) found that an increase in monthly AMSR-E derived SM of 0.045 g/cm^3 resulted in an increase in MODIS emissivity of 10% at 8.55 μm over North Africa during July and August. A more recent, and interesting study by Scheidt et al. (2010) used diurnal surface temperature differences combined with albedo data from ASTER to estimate the apparent thermal inertia (ATI). A case study at White Sands, New Mexico showed that ATI had the potential for monitoring variations in SM, grain size, and sand transport of dune systems.

The LSE plays an important role in surface–atmosphere interactions as well as estimating Earth's surface radiation budget. Surface radiation estimates are in turn used to compute important climate variables such as land surface and air temperature (Zhou et al., 2003). A study by Zhou et al. (2003) found that the broadband soil emissivity (BBE) over semi-arid regions such as Northern Africa and Arabian Peninsula in the window region (8–13.5 μm) are too high (0.96), and

[☆] ©2008 California Institute of Technology. Government sponsorship acknowledged.

^{*} Corresponding author.

E-mail address: glynn.hulley@jpl.nasa.gov (G.C. Hulley).

sensitivity tests using the recently developed Community Land Model (CLM3) (Oleson et al., 2004) indicate that a decrease in emissivity of 0.1 (10%) will result in an increase in LST of 1 °C, and decrease in net longwave radiation of 7 W/m². Using MODIS data, another study by Ogawa et al. (2008) found a wide range of BBE's (8–13.5 μm) over arid regions ranging from 0.86 to 0.96, with maximum variations of 0.03 (3%) at three selected sites which corresponded to increases in AMSR-E derived surface SM. Consequently, SM effects on LSE should be accounted for in order to improve LSE characterization in climate models and minimize errors in model simulated surface temperatures and ground fluxes.

In this study we address the following three important science questions related to the LSE and SM dependence using laboratory measurements and remote sensing observations. Firstly, on what timescale does the LSE reach an equilibrium state after precipitation events? In other words, how long does the bare land surface take to completely dry after wetting, where TIR observations are sensitive to the first few micrometers of the land surface? Secondly, are AIRS, MODIS, and ASTER LST&E retrieval algorithms able to capture LSE variations due to SM changes after precipitation events? And thirdly, what is the magnitude of the LSE increase after precipitation events as observed from space, and how is it correlated to the SM change?

Initially we outline a laboratory experiment to investigate the temporal LSE variation of two water-saturated sand samples in order to simulate a rainfall event. We then investigate SM effects on LSE for an anomalous rainfall event over the Namib Desert in Namibia during April 2006 using three different LST&E retrieval algorithms applied to MODIS data, and the current AIRS standard version 5 retrieval.

2. Laboratory measurements

The variation of LSE with SM should depend on factors such as mineralogy, particle size, and organic matter content of the soil sample (Mira et al., 2007). In this study two sand samples with varying mineralogy and particle size were chosen for analysis. The sand samples were collected from the Great Sands National Park, Colorado, and Coral Pink Sands, Utah in the USA and previously used to validate the North American ASTER Land Surface Emissivity Database (NAALSED) v2.0 (Hulley & Hook, 2009b; Hulley et al., 2009a). X-Ray Diffraction (XRD) measurements showed that the Coral Pink sand was composed of medium-grained pure quartz, while the Great Sands sample contained a mixture of medium-to-coarse grained quartz, feldspar, and magnetite. Neither sample had any clay nor organic matter present and so the particle size difference between the samples would have a negligible effect on SM and LSE dependence. We expect the mineralogy to play a larger role, since the Great Sands samples have darker material consisting of feldspars and magnetite.

2.1. Experimental setup

First, small Petri dishes (1.5 cm height, 6 cm diameter) were filled with sand from Coral Pink (CP) and Great Sands (GS). Water was then added to each sample and allowed to infiltrate until the saturation point was reached, i.e. when all soil pores were filled with water and there was no air left in the soil. The gravimetric method was used to determine the SM content of each sample and is expressed as weight ratio of water present in the sand to the dry weight of the sand sample.

The directional hemispherical reflectance of the water-saturated samples were then measured using a Nicolet 520 Fourier transform infrared (FT-IR) spectrometer with an integrating sphere, and converted to emissivity using Kirchhoff's law. The uncertainty associated with the FT-IR lab emissivity is 0.002 (0.2%) (Korb et al., 1999). Reflectance spectroscopy measurements are more well suited to this study since in emission spectroscopy, samples typically have to be heated to high temperatures (e.g. 80 °C) to improve signal-to-noise

which could change the evaporation rate of the sample. Furthermore, Salisbury et al. (1994) showed that emissivities calculated from lab measurements using reflectance and emittance methods are equally valid, but a measurement of emissivity is far more complex compared to a measurement of reflectance, due to multiple sources of error involved. After each reflectance measurement, the samples were placed outside to dry. Emissivity measurements were subsequently made every hour throughout the day, starting at 8 am, and ending when the dry equilibrium state had been reached, and all SM had evaporated. The lab measurements took approximately 10 min, before samples were taken back outside to dry. Hourly measurements of air temperature, pressure, relative humidity, wind speed, wind gust, and solar radiation were recorded from a meteorological station nearby.

2.2. Results and discussion

2.2.1. Emissivity and soil evaporation relationship

The JPL lab emissivity data were convolved to the ASTER spectral response for band 11 (8.6 μm), and the 8.6 μm emissivity together with the SM measurements and meteorological data are shown in Table 1. The full resolution laboratory spectra ranging from 3 to 13 μm are shown in Fig. 1 for the wet and dry samples from CP and GS. In Fig. 1, the two characteristic quartz doublets are clearly visible for the CP sample between 8–9.5 μm and 12–13 μm. The GS dry spectra have less spectral variation, with emissivities greater than 0.85 in the TIR (8–12 μm) due to the presence of feldspar and magnetite in the samples, as opposed to a greater abundance of quartz in the CP sample. The wet emissivity spectra for both samples are high and spectrally flat in the shortwave infrared (SWIR) region (3–5 μm), and TIR emissivities are approximately 10–15% higher in the quartz reststrahlen band (8–9.5 μm) with similar spectral features as the dry sample spectra. In the longwave 11–12 μm window, emissivity variation with SM is less and ranges from 0 to 3%. It is also interesting to note that the maximum LSE's for both wet and dry samples in the longwave region near 12 μm are the same and independent of SM content.

Fig. 2 shows the temporal LSE change between measurements for CP and GS samples with the lab measurements convolved to ASTER bands 11 (8.6 μm), 12 (9.1 μm), 13 (10.6 μm), and 14 (11.3 μm). The first noticeable observation is that the LSE decreases dramatically by ~0.17 in the 8–9.5 μm range for CP and by 0.05 for GP within the first hour of drying between 9 and 10 am. A second experiment with the CP sand showed that this sharp drop in LSE actually occurs within the first 15 min of drying. The LSE stayed relatively constant during the following 2h until midday, when it decreased further to the dry equilibrium state in the hour following midday.

We hypothesize that the LSE change during the drying process corresponds closely with the well-known three-stage soil evaporation rate process (Idso et al., 1974; Ventura et al., 2006). In the first stage, the evaporation rate is high and determined by the amount of energy available to vaporize soil moisture in the upper layer, and is controlled by atmospheric conditions. Stage 2 is reached when sub-surface soil water cannot be transferred to the surface fast enough to meet the evaporative demand (Idso et al., 1974), and evaporation rates depend on soil hydraulic properties that determine the transfer of water (primarily vapor) to the surface – a process commonly known as wicking. In stage 3 the evaporation rate is small and constant and determined by soil absorption characteristics (Lemon, 1956). These three stages are indicated in Fig. 2. During stage 1, the LSE decreases considerably in the first hour due to rapid evaporation from the top surface layer, while during stage 2 the LSE remains fairly constant and actually increases very slightly by few tenths of a percent (at 12:38 for both CP and GS), most likely due to water (in either liquid or vapor form) being transferred to the surface from the lower layers by a process known as wicking. Once all the water in either liquid or vapor form has been used up, the LSE decreases further by approximately 1%

Table 1
Data from laboratory emissivity measurements at 8.6 μm and 11.3 μm and gravimetric soil moisture measurements for two sand samples, CP (Coral Pink Sands) and GS (Great Sands) taken every hour until the dry state had been reached. Also shown is the atmospheric data every hour taken from the meteorological station at JPL.

	Time	Lab emissivity (8.6 μm)	Lab emissivity (11.3 μm)	Soil moisture (%)	Air temp ($^{\circ}\text{C}$)	Relative humidity (%)	Wind velocity (m/s)	Solar radiation (W/m^2)
CP	9:00	0.888	0.978	16.1	18.9	57.0	0.2	234
	10:02	0.714	0.959	13.4	20.7	42.2	1.1	346
	11:15	0.714	0.959	10.3	22.7	33.6	1.3	433
	12:38	0.716	0.959	7.3	24.0	26.4	0.7	435
	13:56	0.700	0.957	4.0	23.0	32.7	2.2	331
	15:08	0.697	0.959	1.3	21.8	29.6	2.3	199
	16:00	0.694	0.961	0.4	20.5	35.0	1.5	100
	Dry	0.695	0.964	0.0	–	–	–	–
GS	9:13	0.946	0.977	14.8	20.7	50.2	0.5	264
	10:19	0.896	0.950	12.6	20.4	42.7	1.4	370
	11:34	0.898	0.953	9.5	23.0	33.3	1.0	436
	12:58	0.898	0.953	5.9	23.9	28.2	1.5	412
	14:08	0.891	0.950	2.3	23.2	32.9	1.4	315
	15:15	0.887	0.951	0.7	21.8	29.6	2.3	199
	16:20	0.884	0.956	0.3	20.0	35.0	1.5	100
	Dry	0.885	0.953	0.0	–	–	–	–

during stage 3 from hours 5–8 until the equilibrium dry state has been reached. Wind conditions were calm throughout the day (max 2 m/s), so the effects of wind speed on the evaporation rate were probably small, leaving solar radiation as the primary factor for controlling the amount of energy available for evaporation. The maximum air temperature recorded (24 $^{\circ}\text{C}$) coincided with the end of stage one in which the solar radiation was also at a maximum (435 W/m^2).

SM measurements show that the GS sample dried at a faster rate than the CP sample from hrs 3–5 of drying (~11:00–14:00), which could be due to the GS samples consisting of darker material (quartz mixed with feldspar and magnetite), resulting in the sample heating up quicker than the light colored CP quartz grains. Grain size, bulk density, and to a lesser extent organic matter content and porosity are other contributing factors to evaporation rate differences between the two samples.

2.2.2. Sun and shadow experiment

The final lab experiment used a sand sample from the Namib desert in Namibia (Hulley & Hook, 2009a; Hulley et al., 2009b) to

investigate sun and shadow effects on the evaporation rate, and hence LSE change, by placing one sample in direct sunlight, and the other behind an obstacle in complete shade during the drying process. Since we know the kinetic energy of a molecule (e.g. water) is proportional to temperature, we expect the direct solar radiation to increase the evaporation rate due to an increase in temperature of the surface molecules. Both samples were identical in the total mass of sand and water used in each Petri dish. The results are shown in Fig. 3 for ASTER bands 11–14. Once again the sharp drop in LSE can be seen after the first hour with both samples having close to the same LSE at all wavelengths (within 1% at 8.6 μm). Therefore, under these atmospheric conditions, there was sufficient energy to evaporate moisture from the sand surface within the first hour after wetting, regardless of whether the sand was in shade or exposed to direct sunlight. At lower temperatures, however, results may be different. Because of the warm day, with temperatures approaching 30 $^{\circ}\text{C}$, the SM of the sun sample was close to 0% by 1 pm, whereas the SM of the shadow sample approached 0% much later at 4:30 pm.

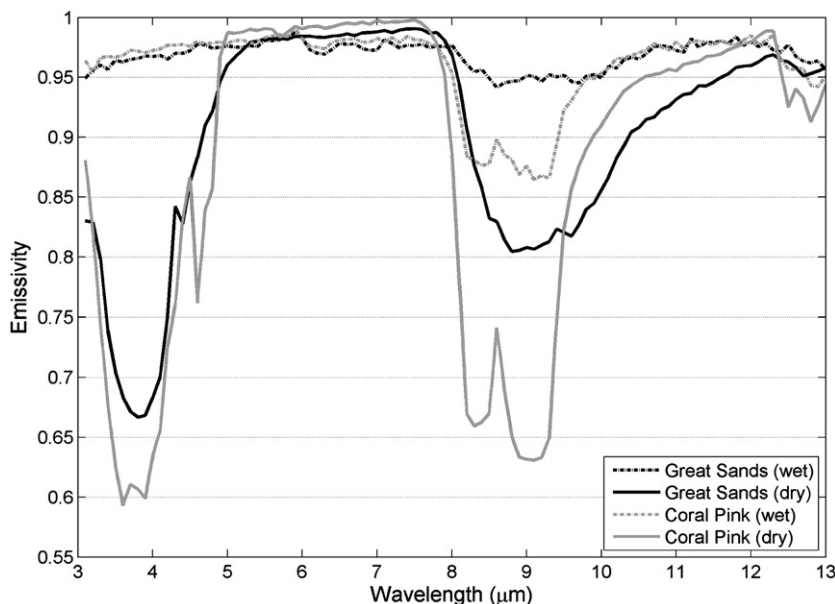


Fig. 1. Laboratory emissivity spectra for a wet (dashed lines) and dry (solid lines) sand sample from Coral Pink Sands, Utah and Great Sands, Colorado.

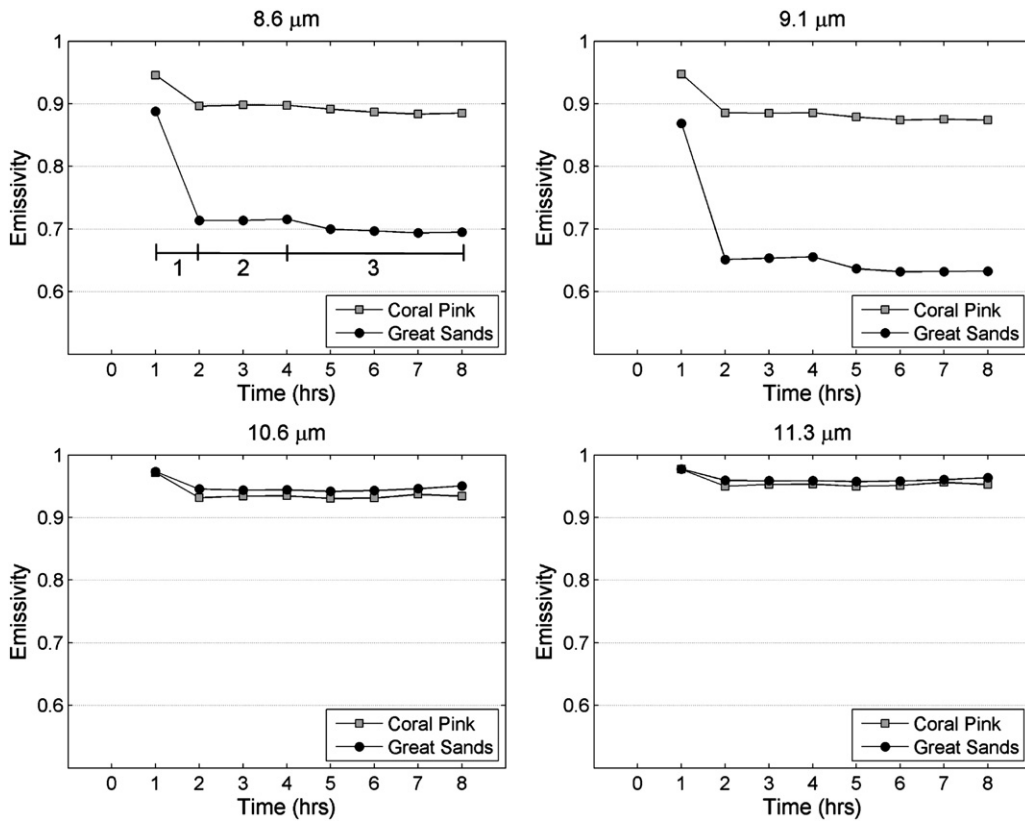


Fig. 2. Laboratory measurements of sand samples from Coral Pink and Great Sands showing the emissivity variation over time starting with a fully saturated sample. The top left panel identifies the three-stage soil evaporation rate process discussed in the text.

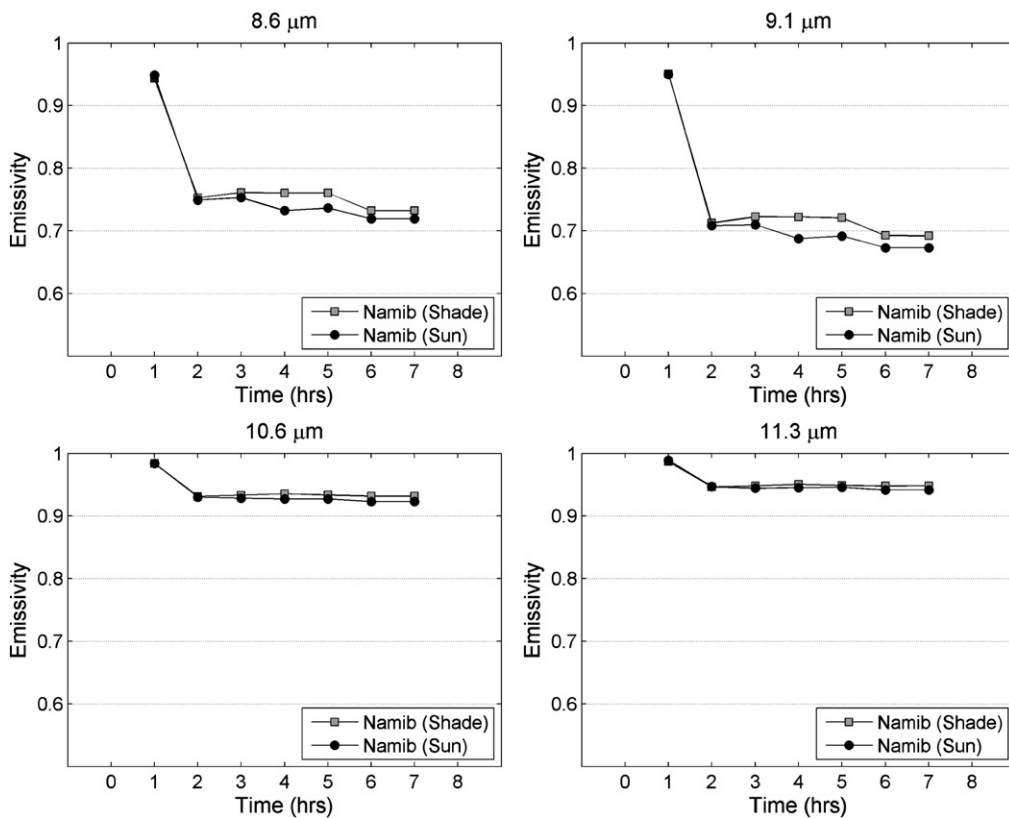


Fig. 3. Laboratory measurements of a sand sample from the Namib Desert showing differences in the emissivity variation over time between a sample left to dry in direct sunlight and the other in shade.

2.2.3. Emissivity spectral unmixing and implications for soil moisture estimation

Using a time series of LSE observations over a given sand dune site (e.g. Coral Pink Sands), we propose a method for estimating the SM from the LSE variations by a technique known as spectral unmixing. Spectral unmixing is the procedure by which a measured spectrum of a mixed pixel is decomposed into a collection of endmember spectra (e.g. sand and water), and a set of corresponding fractions, or abundances, that indicate the proportion of each endmember present in the pixel. For example, Ramsey et al. (1999) used a linear spectral unmixing algorithm combined with spectral library endmember minerals to investigate sand mineralogic variations and transport sources at Kelso Dunes, California.

In this example, we use high spectral resolution lab measurements and assume the two endmembers consist of pure sand (e.g. quartz) and water only. However, in reality spectral unmixing of a mixed scene over a semi-arid area could be problematic due to additional spectrally flat endmembers such as vegetation, and also variations in sand particle size, organic matter content, and mineralogy (e.g. clays, magnetite, and hematite). The problem becomes more difficult when considering multi-spectral satellite data, since less information is available to resolve spectrally similar endmembers. In this case a blackbody (emissivity = 1) could be used as additional endmember which would increase the spectral contrast of satellite measurements which typically have shallower spectra than lab measurements. Currently high spatial and spectral resolution data which would allow a greater number of endmembers are unavailable, but it is likely such data will be available in the future thereby enabling this approach from space.

Fig. 4 shows spectral unmixing results for the GS and CP samples. The unmixing linear least squares problem was solved using QR decomposition. The two endmember spectra (water and dry sand) are shown along with spectra of the saturated sand sample and a fit to the saturated sample using spectral unmixing. For GS, the spectral unmixing results yielded a 19% sand and 81% water contribution and fitted the observed measurement closely with an RMSE of 0.0039. For Coral Pink, the results yielded a 31% sand and 69% water contribution with an RMSE of 0.0048.

The fraction of water in a mixed emissivity spectrum computed from spectral unmixing can be used to estimate the soil moisture by modeling the dependence for a range of different water contents in the laboratory. In this study, we only show the dry and wet (saturated) results for two different sand types, but the approach could be extended to include more sand types in the future.

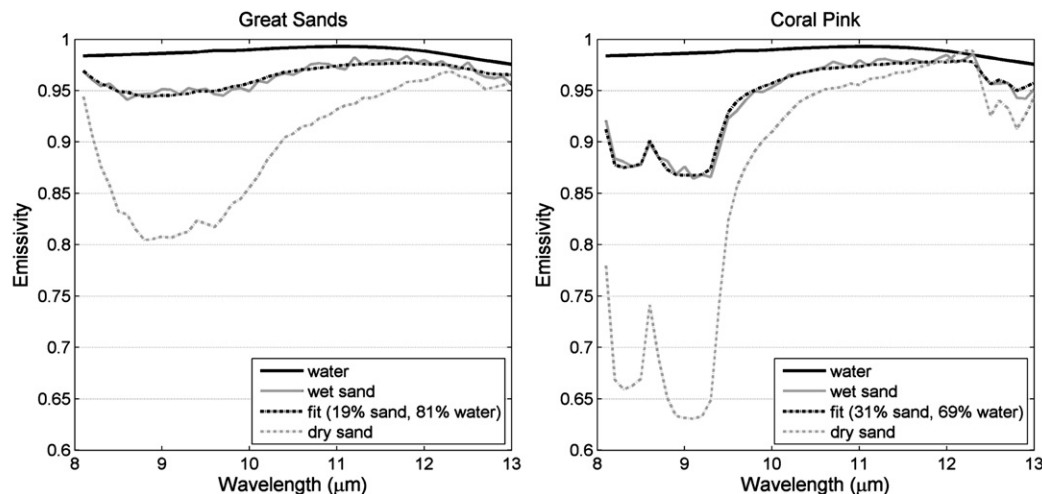


Fig. 4. Laboratory emissivity spectra of water, a fully saturated sand sample, a dry sand sample, and a fit to the fully saturated sample using spectral unmixing for Great Sands (left) and Coral Pink (right).

An application of the technique would be to model the water fraction and SM dependence for sand samples from the Kalahari and Namib desert (Hulley et al., 2009b) in the lab, and then using a series of remote sensing LSE observations, the model could be applied and used to estimate the SM changes corresponding to higher than normal LSE values in the absence of vegetation cover change, or used in combination with NASA's future Soil Moisture Active and Passive (SMAP) mission scheduled for launch in the 2010–2013 time-frame. Determining the spatial and temporal distribution of SM is a key variable both in agricultural land use and degradation processes such as erosion and desertification (Van Der Kwast, 2009). For example, Thomas et al. (2005) showed that global warming in the 21st century over Southern Africa would result in more droughts that could potentially kill off plant and grass species that anchor and stabilize the dunes of the Kalahari Desert. The result would be an increase in dune surface erodibility causing large amounts of sand to become airborne which would kill livestock and potentially threaten the livelihood of millions of people in the surrounding farming areas.

3. Satellite retrievals

The following two sections firstly describe the various retrieval methods used to produce LST&E products from the MODIS and AIRS sensors, and then investigate the underlying source of differences between the methods over the Namib Desert during April 2006, which included a precipitation event toward the end of the month.

The continuous monitoring of multiple product versions and algorithms from different data sources is essential for laying down a baseline quality metric to which future climate datasets and trends can be measured. For example, if two independent algorithms, using either the same or different data sources yield similar results over varying conditions, then a climatology built on either data source can be trusted. If, however, the two datasets diverge, then the trends are suspects.

3.1. AIRS

The AIRS is an infrared spectroradiometer onboard the Earth Observing System (EOS) Aqua satellite that provides high spectral resolution (2738 channels) observations of outgoing thermal infrared emission from the Earth and atmosphere covering the 3.7–15.4 μm range for climate research and weather prediction (Susskind et al., 2003). The current AIRS v5 surface retrieval algorithm uses a regression plus simultaneous solution approach to retrieve skin

temperature and spectral surface emissivity, with the initial regression based on a land surface emissivity model of laboratory measurements (Fishbein et al., 2003). In this paper we use a daily, level-2 product at 45 km spatial resolution with emissivity retrieved at 39 wavelengths from 3.8–15 μm . Each wavelength is defined at a hinge point, which sufficiently captures the spectral shape of any emissivity spectrum. The v5 LSE product has been validated over the Namib and Kalahari deserts in a previous study using ASTER data and laboratory measurements (Hulley et al., 2009b).

3.2. MODIS

The Moderate Resolution Imaging Spectroradiometer (MODIS) is a multi-spectral imager onboard the Terra and Aqua satellites of NASA's Earth Observing System (EOS), and has been the flagship for land surface remote sensing since the launch of Terra in December 1999. MODIS LST&E standard products (MOD11 from Terra, and MYD11 from Aqua) are generated by two different algorithms: a generalized split-window (GSW) algorithm (product MOD11A1) and a physics-based day/night algorithm (product MOD11B1). In addition we apply the ASTER Temperature Emissivity Separation (TES) algorithm to MODIS data as an independent source of comparison.

3.2.1. Day/night algorithm

The day/night algorithm is a physics-based algorithm produced in the MOD11B1 product which solves the ill-posed TIR problem by assuming the LSE stays constant during daytime and nighttime observations, while retrieving two surface temperatures (Wan & Li, 1997). Using 14 pieces of information (day/night pairs for MODIS bands 20, 22, 23, 29, and 31–33), 2 day/night LST's, 7 emissivities, 2 water vapor profiles, 2 air temperature profiles and one asymmetric factor are solved for using a statistical regression and least squares method.

In version 4 (v4) of the MOD11B1 product, the day/night algorithm partially incorporates the GSW method (Wan & Dozier, 1996) and is generated on a sinusoidal projection with a spatial resolution of 5 km (exactly 4.63 km). In version 5 (v5), the day/night algorithm is fully incorporated with the GSW (Wan, 2008) with a spatial resolution of 6 km (exactly 5.56 km). The initial values of emissivities in band 31 and 32 from the GSW method, total column water, and air temperature, are used as iterators in the solution of the day/night algorithm. The tighter coupling of the GSW with day/night algorithm in v5 has led to LSE's being overestimated in arid regions (LST underestimated), and as a result an interim MOD11B1 product version, termed version 4.1 has been generated, which uses the v4 algorithm with v5 input products, and is currently being produced as a continuation of the v4 data (Hulley & Hook, 2009a).

The day/night algorithm has been validated with in-situ measurements for six cases in Railroad Valley and one case of snow cover in Bridgeport, CA, and LST's agreed to within 1 K, but have a large uncertainty due to the 5-km grid resolution (Wan et al., 2002). This method is susceptible to cloud effects from nighttime observations, and also may be inaccurate if the daytime and nighttime LSE are in fact different, due to SM changes from rainfall or early morning dew accumulation for example.

3.2.2. Generalized Split-Window (GSW) algorithm

The GSW algorithm is produced in the MOD11A1 product and extends the SST split-window to land surfaces using the assumption that a wide range of land cover types have stable emissivities in the 10.5–12.5 μm wavelength range, which fall within MODIS bands 31 and 32. The emissivity of these land cover types can then be classified *a priori*, and a split-window technique applied as before with oceans (Wan & Dozier, 1996). This algorithm is stable over densely vegetated areas and water, but will be less accurate over semi-arid and arid regions where the LSE's are more uncertain. Also, the GSW algorithm

will have problems in retrieving accurate surface temperatures over areas affected by surface SM, due to changes in the longwave LSE.

3.2.3. ASTER Temperature Emissivity Separation (TES) algorithm

ASTER was launched on the Terra satellite in December 1999, and has five spectral bands in the TIR (8–12 μm) with a spatial resolution of 90 m. The standard surface temperature and emissivity products for ASTER are generated by the Temperature Emissivity Separation (TES) algorithm (Gillespie et al., 1998). TES uses surface emitted TIR radiance data as input, which has been atmospherically corrected for atmospheric transmission and path radiance. The downward sky irradiance, an output of the atmospheric correction, is removed iteratively. The ill-posed problem of separating temperature and emissivity in TES is then solved by using an empirical relationship to predict the minimum emissivity that would be observed from a given spectral contrast, or minimum–maximum difference (MMD) (Kealy & Hook, 1993; Matsunaga, 1994). The empirical relationship is referred to as the calibration curve and is derived from a subset of spectra in the ASTER spectral library (Baldrige et al., 2009). In this study the TES calibration curve is modified for MODIS bands 29, 31, and 32 and is computed from spectra of 90 different terrestrial materials consisting of different rocks, soils, vegetation, snow, and water from the ASTER spectral library and sand samples used in validating the NAALSED (Hulley et al., 2009a). The resulting MODIS calibration curve is given by

$$\varepsilon_{\min} = 0.950 - 0.7503 \cdot \text{MMD}^{0.8321}$$

where ε_{\min} is the minimum emissivity for all three bands, and MMD is the difference between the minimum and maximum difference. Using ε_{\min} , the full emissivity spectrum can then be recovered from the emissivity band ratios.

TES is designed to retrieve accurate emissivities of mineral substrates for applications of mineral mapping and resource exploration. A validation campaign over nine sand dune sites in the southwestern USA showed that TES retrieves emissivity to within 0.016 (1.6%) for a wide range of emissivities in the TIR (Hulley et al., 2009a). A further advantage of TES is that it produces seamless images with no step discontinuities, as might be introduced if a land classification type algorithm was used.

The limiting factor on TES performance is the accurate calculation of the atmospheric transmissivity and path radiance. Errors of more than 2 K can be expected in humid conditions if the water vapor content is not well characterized, and errors could be larger over gray body surfaces where the calibration curve is particularly sensitive to errors in atmospheric compensation (Gillespie et al., 1998). The TES algorithm applied to MODIS data will from now on be referred to as the MODTES product.

4. Namib Desert rainfall event

The following case study looks in detail at an anomalous rainfall event over the Namib Desert in Namibia during April, 2006. The prime objective of this study is to investigate the underlying source of differences between the respective LST&E retrieval methods described above, and to better understand the LSE/SM dependence using additional SM and rainfall observations from the AMSR-E and TRMM sensors.

4.1. The Namib Desert

The Namib Desert in Namibia is bordered to the north by the Kuiseb River, the south by the Orange River, the west by the Atlantic Ocean, and the east by the South African escarpment, and forms part of the Naukluft–Namib National Park that occupies some 34,000 km² and comprises some of the oldest (~55 million years) and highest (up

to 300 m) dunes in the world. The Namib is a hyper-arid ecoregion and receives a low and highly unpredictable annual rainfall of between 5 mm in the east and 85 mm in the west (Lovegrove, 1993). A combination of sub-tropical subsidence from the Hadley Cell and cool coastal sea surface temperatures (SSTs) from the Benguela current result in one of the driest deserts in the world, where the vast expanse of shifting dunes are almost completely devoid of vegetation except for sparse perennial grasses (White, 1983).

For the week of 16–22 April 2006, the Namib Desert experienced an anomalous rainfall event where more than 100 mm of rain was recorded within one week at the coastal town of Luderitz — six times the long-term annual rainfall average of 16.7 mm (Muller et al., 2008). Wet conditions over Southern Africa during this time resulted from a combination of La Niña event and warming of the southeast Atlantic Ocean. Daily rainfall data from the Namibian Meteorological Service showed that Luderitz received 39.4 mm of rain on the 16th, 20 mm on the 19th, 27.4 mm on the 20th, 11.2 mm on the 21st, and 2.6 mm on the 23rd (Muller et al., 2008).

4.2. TRMM and AMSR-E observations

Precipitation data from the Tropical Rainfall Measuring Mission (TRMM; <http://trmm.gsfc.nasa.gov>) were used to analyze the spatial and temporal variations in rainfall over the Namib Desert during the April 2006 rain event. TRMM precipitation estimates are provided on a $0.25^\circ \times 0.25^\circ$ global grid from 50° N to 50° S with three-hourly estimates (UTC) of precipitation (mm/h) during a given day. For this analysis we used the TRMM-calibrated merger product that uses all TRMM Microwave imager (TMI), AMSR-E, AMSU-B and SSM/I precipitation estimates.

Daily level-3 SM estimates (g/cm^3) from the Advanced Microwave Scanning Radiometer (AMSR-E) on Aqua (Njoku et al., 2003) were extracted over the Namib area for the month of April 2006 in order to

observe any correlations with the LSE variation and TRMM rainfall estimates. The level-3 AMSR-E product (AE_Land3) is resampled to a global cylindrical 25 km Equal-Area Scalable Earth Grid (EASE-Grid) cell spacing and available from the National Snow and Ice Data Center (NSIDC). The C-band ($\sim 4\text{--}8$ GHz) is most sensitive to SM, but only in regions of low vegetation cover (Njoku et al., 2003). Since the observation site chosen in this study is over sparsely vegetated dunes in the Namib, we expect surface roughness and vegetation effects on SM retrievals to be limited (Njoku & Chan, 2006).

4.3. MODIS analysis

4.3.1. Study site selection

The first step in investigating the LSE and SM relationship involved pin-pointing areas that received heavy rainfall over the Namib during the April anomalous event, and then looking for correlations between LSE and SM observations over those areas.

Fig. 5 shows the TRMM total accumulated rainfall anomaly (mm) over Namibia for the month of April, relative to the 2006 annual mean rainfall. The anomaly image shows that heavy rainfall during April 2006 was confined to the coast of Namibia and up to ~ 50 km inland in the north and southern parts ($10\text{--}30$ mm), and also parts of north-west South Africa (~ 20 mm). The TRMM results agree well with rainfall anomaly estimates during April 2006 from the International Research Institute for Climatology and Society (IRI) in both magnitude and spatial extent (Muller et al., 2008).

Water is strongly absorbing in the quartz reststrahlen band ($8\text{--}9.5$ μm), and so we expect MODIS band 29 (8.55 μm) LSE to be the most sensitive to changes in soil moisture. Fig. 6 (left panel) shows the mean MODIS v4 LSE for the month of April, 2006 over Namibia using the MOD11B1 tile, h19v11. The Namib Desert can be seen as an area of low LSE ($0.7\text{--}0.8$) bordering the coastal region from Luderitz

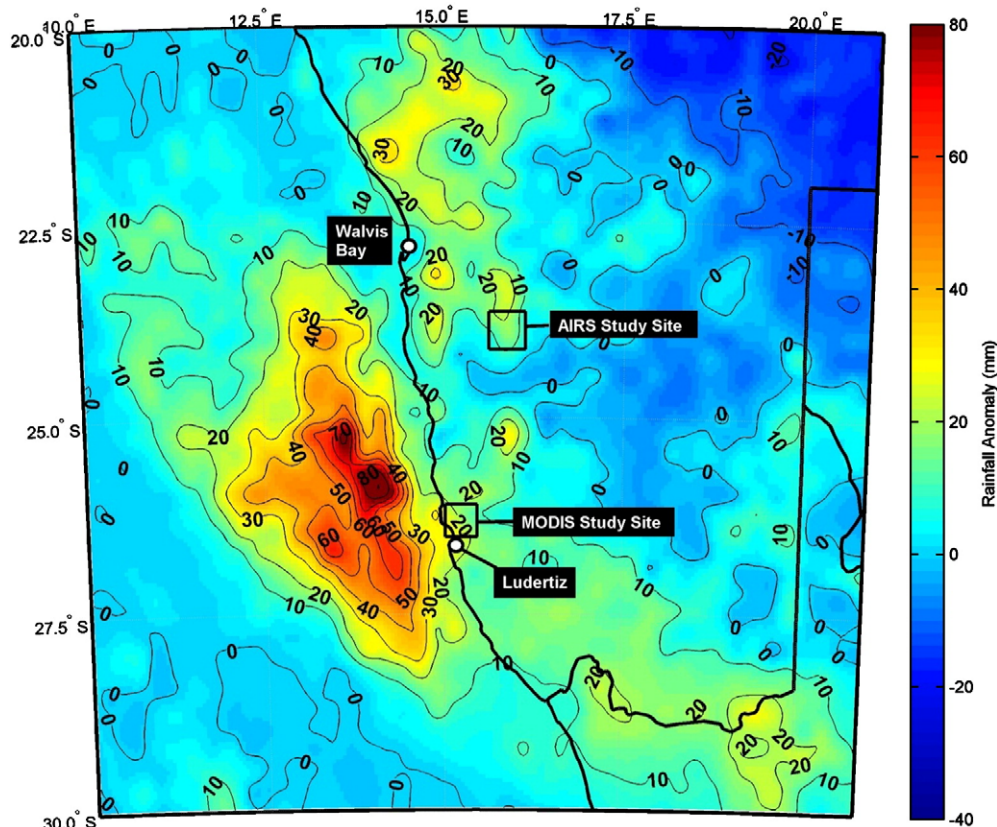


Fig. 5. Tropical Rainfall Measuring Mission (TRMM) rainfall anomaly (mm) for April 2006 with respect to the mean rainfall for 2006 over the Namib Desert, Namibia. Meteorological stations at Luderitz and Walvis Bay are shown for references, along with the MODIS and AIRS study sites chosen for the emissivity analysis.

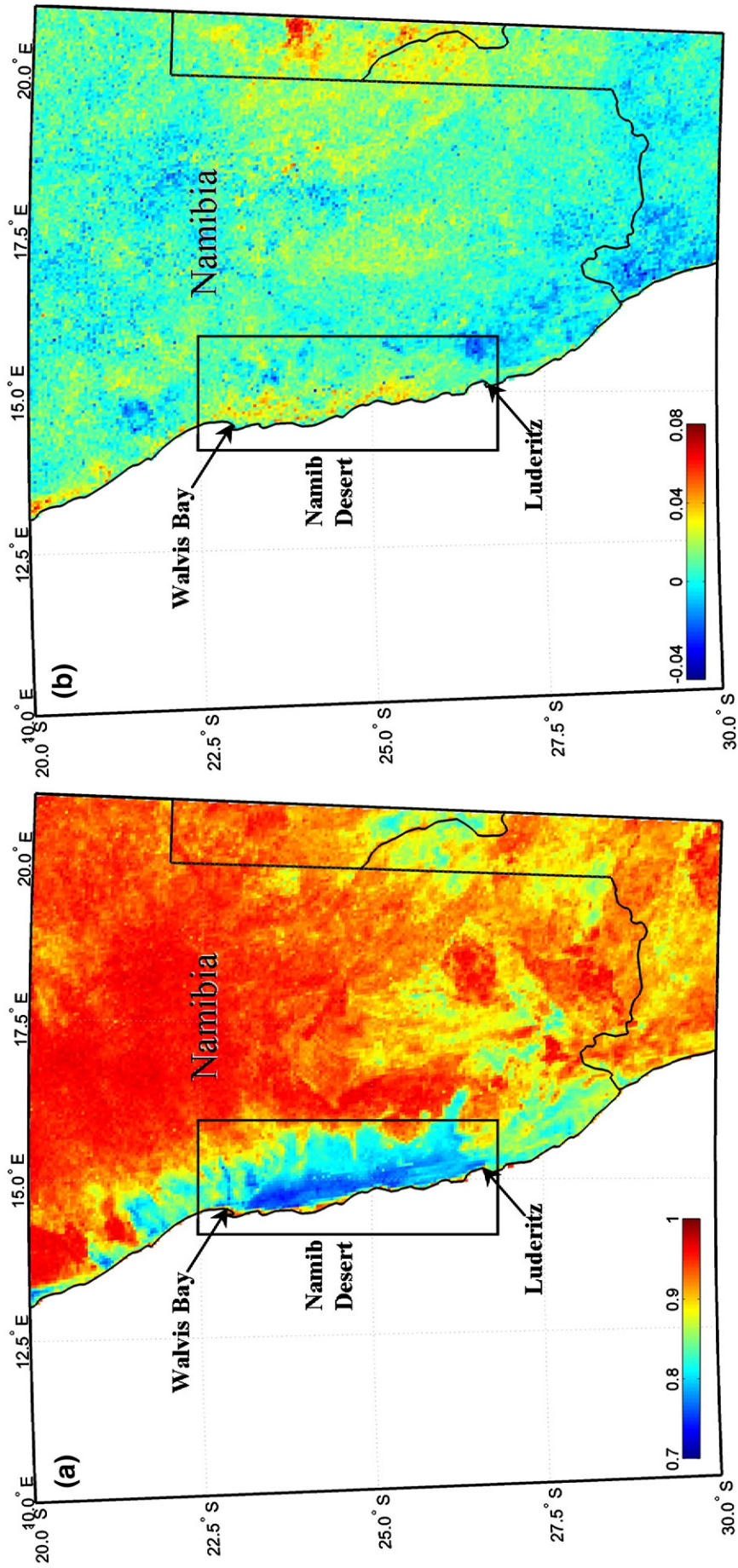


Fig. 6. MODIS band 29 (8.55 μm) mean emissivity for April 2006 using the MOD11B1 v4 product (left panel), and MODIS emissivity anomaly for April 2006 with respect to the mean 2006 emissivity (right panel).

in the south to Walvis Bay in the north. Fig. 6 (right panel) shows the MODIS band 29 LSE anomaly for the month of April, relative to the 2006 annual mean LSE. Positive anomalies of between 2 and 6% in LSE can be seen along the coast of the Namib Desert to within 50 km inland which agrees well with positive rainfall anomalies from TRMM. Large positive LSE anomalies along the Botswana western border are most likely a result of seasonal vegetation cover changes after rainfall events.

Using the TRMM rainfall and MODIS LSE anomaly map as a guide, an area just north of Luderitz (26–26.5° S, 15.1–15.4° E) corresponding to ~60 MODIS 5 km pixels were selected for the MODIS analysis, with the area indicated in Fig. 5.

4.3.2. Emissivity results

The TES algorithm was first used to retrieve temperature and emissivity using The MODIS Level-1B calibrated radiance product, MOD021KM for all granules covering the study area during the month of April, 2006. The MODIS L1B radiances were first atmospherically corrected using a new state-of-the-art MODTRAN 5 radiative transfer model with spectral resolution down to 0.1 cm⁻¹ (Berk et al., 2005), and input atmospheric profiles of temperature, humidity, and geopotential height from the MODIS joint atmospheric product (MOD07). The surface radiance and downwelling sky irradiance were then input to the TES algorithm to generate the surface temperature and emissivity products. The MODTES output at 1 km resolution was aggregated to 5 km resolution and geolocated with the MOD11B1 product using the MODIS reprojection tool. To eliminate cloud contamination and bad quality data, Quality Control (QC) information included with the MOD11B1 product (MODIS LST Users guide, 2006) were used to remove observations if the LST was not produced due to cloud effects, or the LST was affected by nearby cloud or ocean.

Fig. 7 shows the MOD11B1 (day/night algorithm) v4 and v5 as well as MODTES (TES applied to MODIS) temporal LSE change for bands 29, 31 and 32 during April 2006, and the corresponding temporal change in AMSR-E derived SM and TRMM rainfall. TRMM data indicated light rainfall on the 4, 7, and 15th, while harder rain fell on the 16th (10 mm), 19th (40 mm), and 20th (36 mm). There is a clear pattern of elevated SM after these precipitation events reaching a maximum of 0.12 g/cm³ on the 22nd – an increase of ~0.08 g/cm³ from the dry observation on the 6th. Similar strong SM and rainfall correlations between AMSR-E and TRMM have been found in West Africa by Pellarin et al. (2008) and in Australia by Draper et al. (2009). One interesting observation is that the AMSR-E increase in SM response time appears to be on the order of 1–2 days after the precipitation events. For example, rainfall on the 16th resulted in elevated SM only on the following day, and heavy rainfall on the 19 and 20th resulted in elevated SM two days later on the 22nd. Given that AMSR-E microwave observations are sensitive to the top centimeter or less of the surface layer, and rapid infiltration of surface water over this type of desert sand environment, one would expect the response time to be much faster. As a result, this could be less of an observational and more of an underlying algorithm issue. TIR and microwave observations do not correlate well during the rainfall events. For example, on the 22nd, the SM observed by AMSR-E reached a maximum of 0.12 g/cm³ for the month, but the MODIS LSE's for MOD11B1 v4 and MODTES were dry and around 0.8. This is primarily because TIR observations are sensitive to the top few micrometers of the surface layer, which dries much faster than microwave penetration depth of around one centimeter. Further work is required to develop a suitable quantitative relationship between TIR derived LSE and microwave retrieved SM from remote sensing observations.

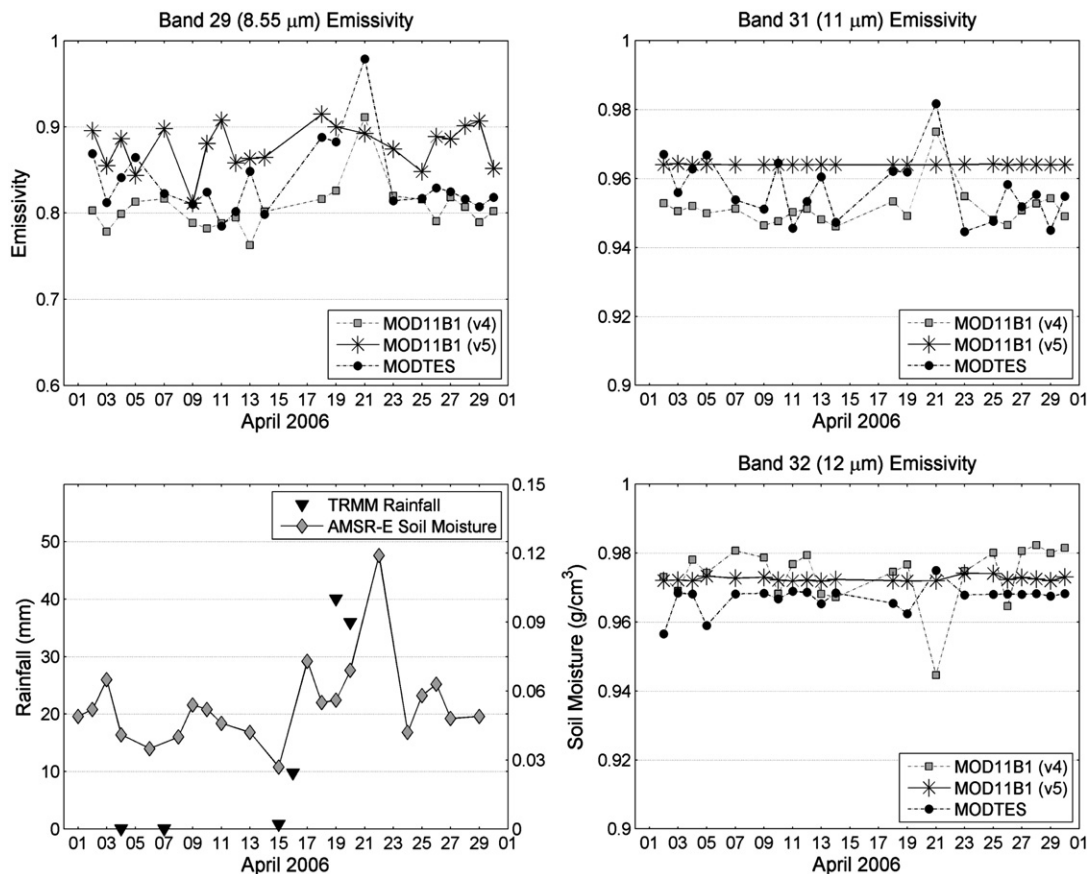


Fig. 7. Temporal emissivity variations of MODTES, MODIS v4 and v5 LSE for bands 29 (8.55 μm), 31 (11 μm) and 32 (12 μm) during April 2006 over the Namib Desert, Namibia. TRMM rainfall estimates and AMSR-E derived soil moisture are shown at bottom left for comparisons.

4.3.2.1. MODTES. The MODTES band 29 (8.55 μm) LSE showed a strong correspondence with the rainfall events on the 19th (40 mm) and 20th (36 mm) with an increase in LSE up to 0.98 on the 21st. This is an approximate 0.015 (15%) increase in LSE when compared to the dry observations during the rest of the month. The LSE then decreases back to just above 0.8 two days later on the 23rd, and remains at this level for the rest of the month. The band 31 results show some variability during the first two weeks, with mean LSE of ~ 0.95 , before increasing above 0.98 after the rainfall event, similar to the band 29 results. The band 32 results are relatively stable during the month around 0.97, with a much smaller increase ($<0.5\%$) after the rainfall events.

4.3.2.2. MOD11B1 v4. The MODIS v4 band 29 LSE results were stable around 0.8 for the first two weeks, before showing an increase in LSE up to 0.91 on the 21st, similar to the MODTES results. MODIS v4 band 31 showed a similar increase in LSE on the 21st as the MODTES result, and interestingly a decrease in LSE or 3% after the rainfall event on the 21st. The assumption of the LSE not changing between day and nighttime could have been violated in the day/night algorithm in this case, resulting in errors in the spectral shape.

4.3.2.3. MOD11B1 v5. MODIS v5 retrieved LSE showed little, or no correlation with SM or rainfall events for the April 2006 period, in all bands. The v5 band 29 LSE's appear to be higher than the MODTES and v4 results, by up to 10% in some cases. The band 31 and 32 results were stable and constant throughout the month, with no variation after rainfall events. In the MODIS v5 product, the day/night retrieval is fully incorporated with the GSW algorithm which fixes band 31 and 32 LSE values depending on the land cover type. As a result, the accuracy of the derived MODIS v5 LSE is degraded over arid and semi-arid regions where LSE variations can be large, both spectrally and spatially (Hulley & Hook, 2009a), and can vary depending on the SM content. A similar split-window/land classification scheme is planned for use in the LST&E products from the NPOESS Visible Infrared Imager Radiometer Suite (VIIRS) sensor (Yu et al., 2005), and will likely yield equally problematic results over arid regions, and when surface conditions change due to surface SM.

4.3.3. Emissivity validation

The LSE results from the three different MODIS retrievals were validated with laboratory measurements of sand samples collected at Sossusvlei in the Namib Desert during July 2008. Details of the sampling site, sand mineralogy and particle size are discussed in Hulley et al. 2009b. Even though the sampling site and the study site in this paper are in different locations, we expect the LSE results to be similar since the coefficient of variation in LSE using a number of ASTER scenes over the Namib was found to be small and less than 1% (Hulley et al., 2009b), indicating the Namib dunes are for the most part homogeneous in LSE. The directional hemispherical reflectance of the eight samples collected were measured in the lab at JPL using a Nicolet 520 Fourier transform infrared (FT-IR) spectrometer, and converted to emissivity using Kirchhoff's law. The uncertainty associated with the FT-IR lab emissivity is 0.002 (0.2%) (Korb et al., 1999). Fig. 8 left panel shows dry emissivity spectra of MOD11B1 (v4 and v5), MODTES and lab results using dry observations from the 23 to the 29th of April. The right panel shows emissivity spectra for the wet observation on the 21st of April. In order to simulate the wet conditions on the 21st, the lab measurement was performed by wetting one of the sand samples to saturation point. For the dry observations, MODTES most closely match the lab results with a combined mean absolute difference in all bands of 0.8%, followed by MOD11B1 v4 with 1.0% and v5 with a 1.8% difference. For the wet observation the MODTES difference was 0.7%, while MOD11B1 v4 was higher at 2.8%. Unfortunately LSE was flagged as bad data on this day for the MOD11B1 v5 product. It is interesting to note that all three measurements show a decrease in emissivity from band 31 to 32, which appears to be overestimated in the MOD11B1 spectra. Also, the MODTES spectra are spectrally flat and very similar to a water spectrum, indicating that there could have been standing water over parts of the dune study site on that day.

4.3.4. Broadband emissivity results

Accurate estimation of the TIR broadband emissivity (BBE, 8–13.5 μm) is essential for determining the surface radiation budget in climate models (Zhou et al., 2003). A study by Ogawa et al. (2008) found that the BBE typically varies between 0.86 and 0.96 in arid regions with small seasonal fluctuations of less than 0.01 (1%) in

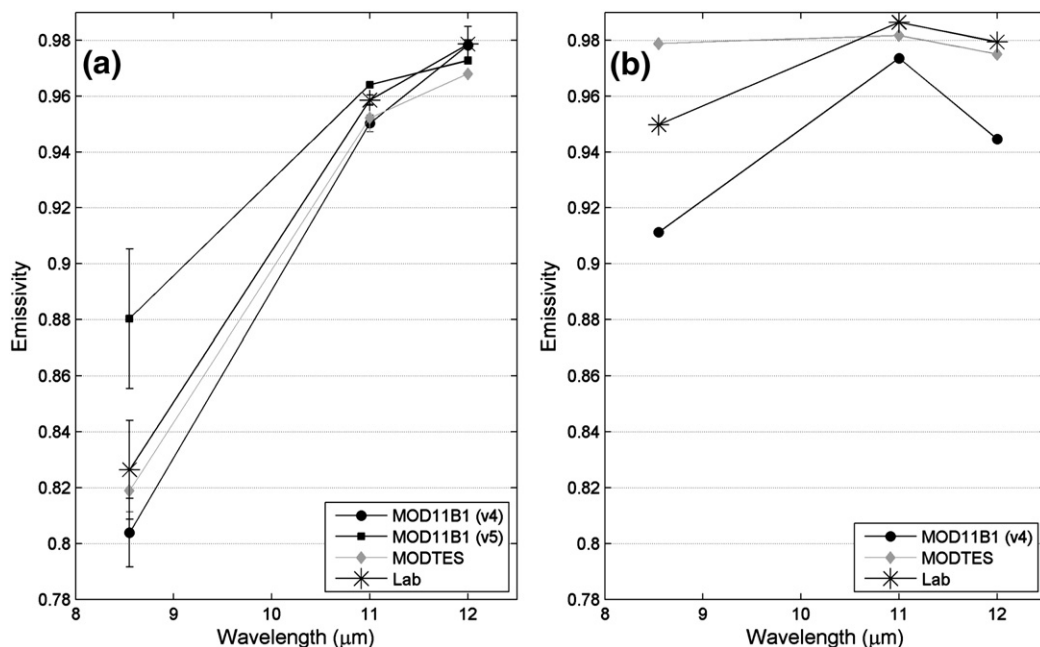


Fig. 8. Mean and standard deviation in LSE for (a) 7 dry observations (23–29th) and (b) one wet observation (21st) over the Namib Desert MODIS study site for MODTES, MOD11B1 v4 and v5 products during April 2006. Note: MOD11B1 v5 retrieval was labeled as poor quality on the 21st, and so the emissivity was set to a fill value in the final product.

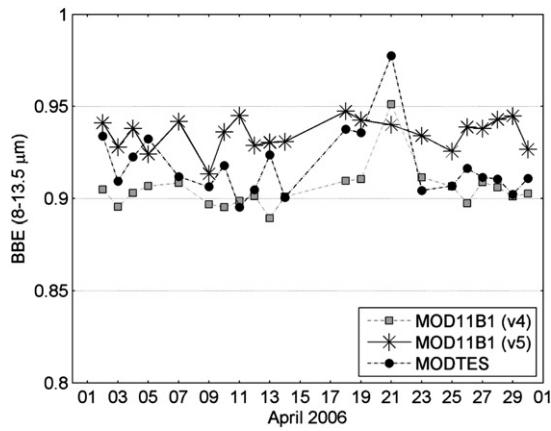


Fig. 9. Temporal variation in the broadband emissivity (BBE) over the Namib Desert MODIS study site for MODTES, MOD11B1 v4 and v5 products during April 2006.

standard deviation. At a few study sites however, the BBE increased by up to 0.03 (3%) which was qualitatively related to changes in surface SM. Using the regression relationship developed in (Ogawa et al., 2008) for estimating BBE from MODIS data, we computed the BBE for the MOD11B1 and MODTES emissivity products for April 2006 shown in Fig. 9. The MODTES and MOD11B1 v4 results showed a distinct increase in BBE of up to 0.07 (7%) and 0.05 (5%) respectively on the 21st after rainfall from previous days. These BBE increases are equivalent to approximately 4.6 W/m^2 and 2.4 W/m^2 changes in net longwave radiation using the flux/emissivity sensitivity relationships derived in Zhou et al. (2003). These values are significant when considering that the current radiative forcing due to an increase in Greenhouse gases is on the order of $2\text{--}3 \text{ W/m}^2$.

4.3.5. Land Surface Temperature (LST) results

Fig. 10 shows the LST variation during April 2006 over the study site for four different retrieval algorithms: the MOD11B1 (v4 and v5), MOD11A1 which is generated using the GSW algorithm, and the

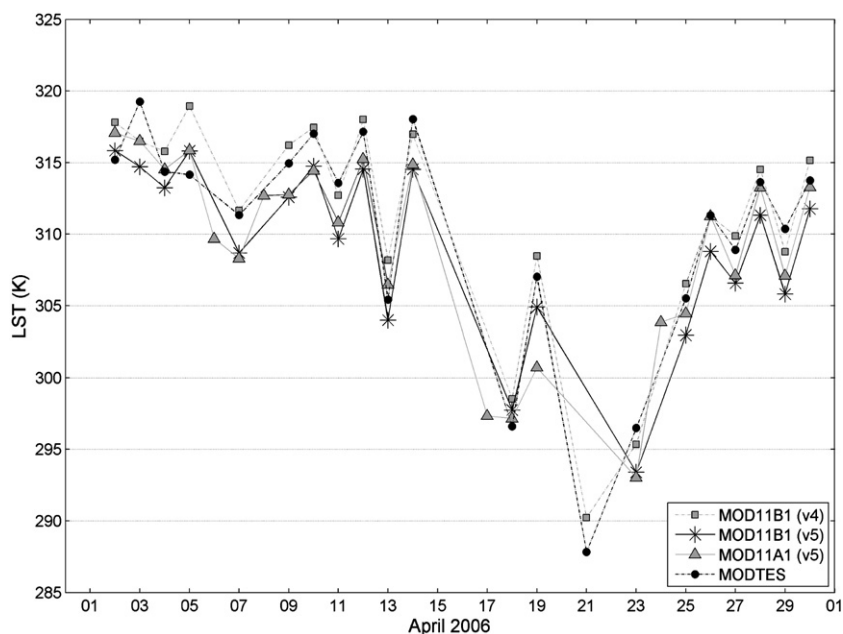


Fig. 10. Temporal variation in the land surface temperature (LST) for the MOD11B1 v4 and v5, MOD11A1 and MODTES products over the Namib Desert MODIS study site during April 2006.

MODTES product. The LST varied between 308 and 320 K for the first two weeks before a sharp decrease to 298 K on the 18th, and 290 K on the 21st due to rainfall on previous days. The LST then increased back up to values above 305 K for the rest of the month as the surface gradually dried out.

Scatterplots of the MODTES versus the standard MODIS LST products in Fig. 11 show that MODTES and MOD11B1 v4 results match the closest with an R^2 of 0.96 and mean LST bias of -0.8 K , even though there is some scatter at higher temperatures. The MOD11B1 v5 and MOD11A1 results show consistently cooler temperatures than the MODTES results with mean biases of 2.1 K and 1.5 K respectively. This is largely because the LSE's are over-estimated in the MOD11B1 v5 product as was shown in Figs. 7 and 8. The good agreement between MODTES and MOD11B1 v4 LST is an interesting result because they were generated by two completely independent retrieval algorithms which give confidence in the results of these two products in the absence of any real validation.

4.4. AIRS analysis

The Luderitz site could not be used to evaluate AIRS because of its much larger field of regard (FOV, $\sim 45 \text{ km}$) than MODIS, and also because of cloud clearing issues over mixed land types in close proximity to the coastline. As a result, a second site was chosen further inland in the northeastern corner of the Namib dunes at approximately 24.5° S , 15.5° E which also showed heavy rainfall during the April 2006 period (Fig. 5 anomaly map).

Fig. 12 shows the resulting AIRS retrieved LSE at $8.6 \mu\text{m}$, SM (AMSR-E) and TRMM temporal variations for the April 2006 period. Up until the 15th, the AIRS LSE and AMSR-E derived SM were relatively stable with mean values of 0.77 ± 0.09 and $0.066 \pm 0.008 \text{ g/cm}^3$ respectively. The AIRS LSE are in good agreement with lab results of a dry Namib sand sample (emissivity of 0.75) with a difference of $\sim 2\%$, a result consistent with AIRS v5 validation results over the Namib desert discussed in Hulley et al. (2009b). TRMM indicated rainfall of 1 mm and 19 mm on the 15th and 16th respectively, which caused a significant increase in the AIRS retrieved LSE with a value greater than 1.0 on the 17th. This unphysical value is a result of the

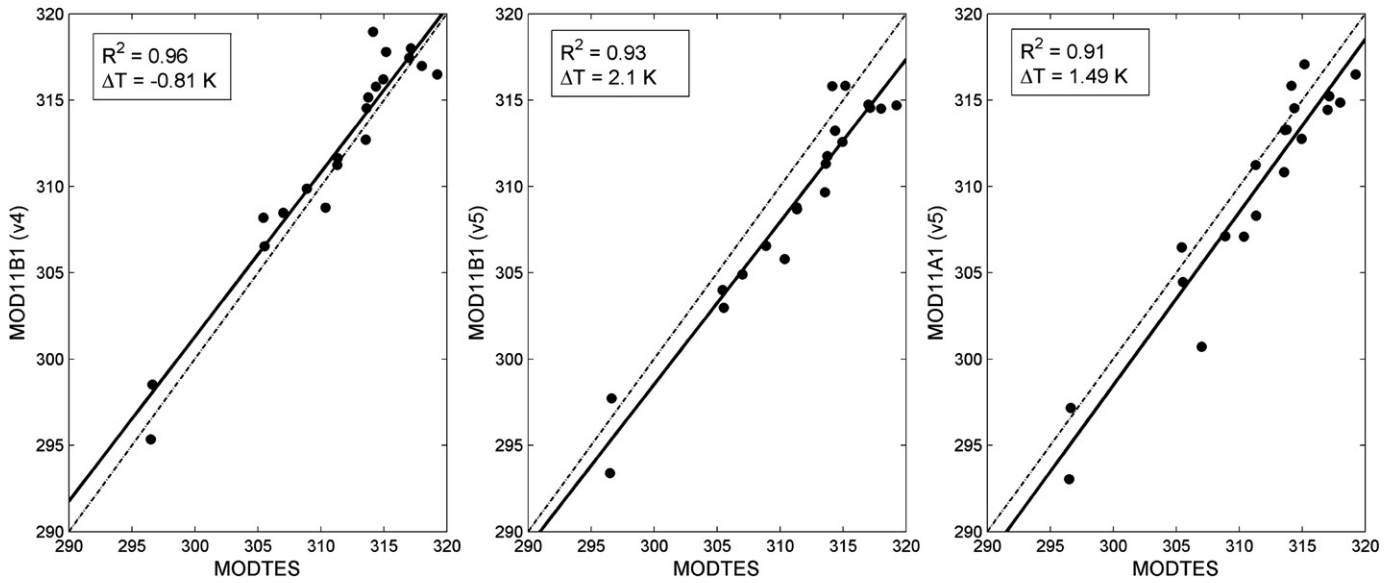


Fig.11. Land surface temperature (LST) scatterplots between MODTES and MOD11B1 v4 and v5, and MOD11A1 products during April 2006 over the Namib Desert MODIS study site.

AIRS LSE being retrieved along with an approximation of associated errors in order to give an unbiased estimate. As a result, AIRS retrieved LSE is limited to be less than 1.05, instead of 1.0. Nevertheless, this result still shows that the AIRS LSE retrieval algorithm is sensitive to changes in SM, and in v6, the unphysical values will be mitigated (Susskind & Blaisdell, 2008). TRMM cumulative rainfall on the 19th was 20 mm, although rain showers started early evening (18:00 UTC, 20:00 local), with a result that the AIRS LSE observation earlier in the afternoon pass was still dry (~0.75). The LSE increased again on the 20th by as much as 15% due to rainfall on the 20th (18 mm). On the

26th, the LSE had reached dry equilibrium state again of approximately 0.75. Similar to the Luderitz site, there is clear pattern of elevated AMSR-E derived SM subsequent to each rainfall event with increases of 0.3 and 0.02 g/cm³ on the 17th and the 22nd.

5. Conclusions

The goal of this study was to better understand the soil moisture (SM) and land surface emissivity (LSE) dependence using laboratory and remote sensing measurements, and to investigate the underlying

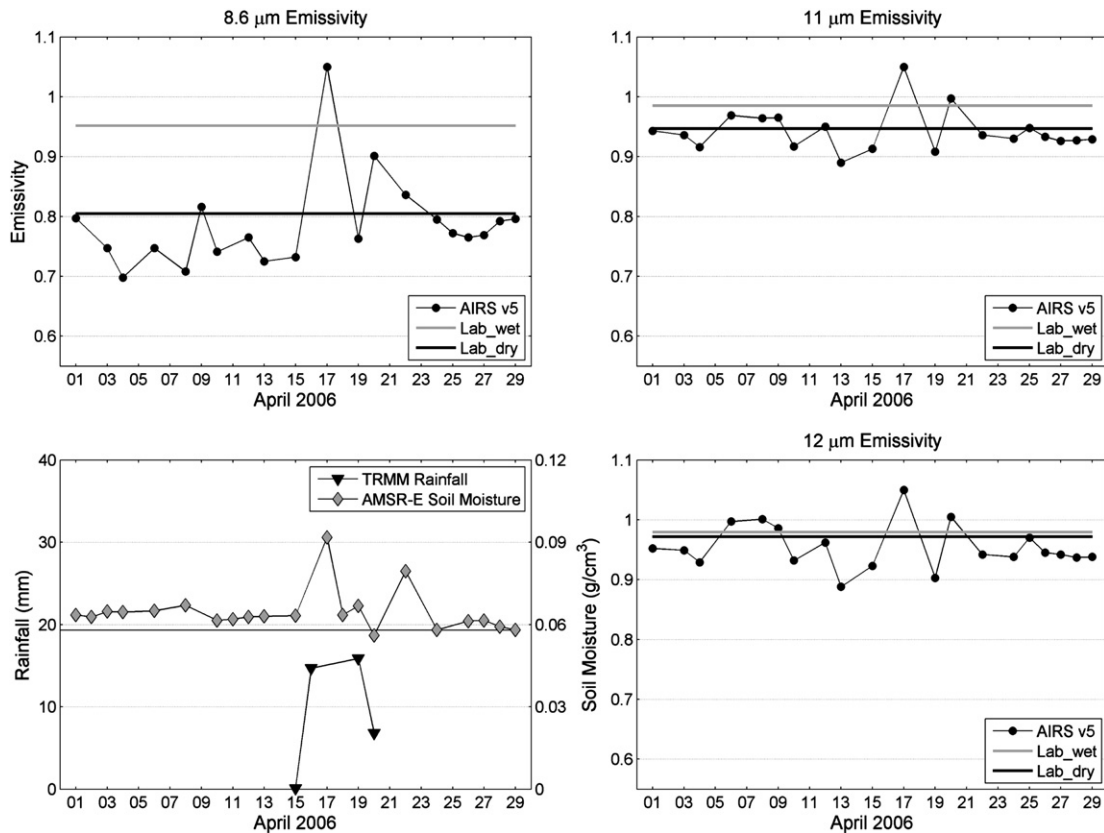


Fig. 12. Temporal emissivity variations of AIRS v5 LSE at 8.6, 11 and 12 μm during April 2006 over the Namib Desert, Namibia. TRMM rainfall estimates and AMSR-E derived soil moisture are shown at bottom left. Wet and dry lab measurements of Namib sand samples are shown as reference.

source of differences between current LST&E retrieval methods from the MODIS and AIRS sensors for an anomalous rainfall event over the Namib Desert in Namibia during April 2006.

Laboratory measurements showed that the LSE at 8.6 μm of two different sand sources increased by 0.17 (17%) for Coral Pink Sands and 0.05 (5%) for Great Sands after wetting and returned to within 1% of the dry equilibrium state within one hour of drying. Since this was a controlled experiment in which the total water content in each sample was limited by the size of the Petri dish, under real conditions, SM in the top surface layer may persist for longer periods of time due to factors such as intensity and length of rainfall events, atmospheric conditions, increased organic matter content, and grain size. In the longwave 11–12 μm window, LSE variation with SM was less and did not exceed 3%. The LSE change from a fully wet state to the dry state was found to be qualitatively related to the well-known three-stage soil evaporation rate process, even although the SM changes throughout the drying process were relatively constant and uncorrelated with the LSE change. Lab measurements also showed no significant LSE variation with SM between sand samples exposed to direct sunlight, and sand samples left in the shade during the drying process. This indicates that direct solar radiation was not the limiting factor on the evaporation rate for the atmospheric conditions in this case. Using a linear spectral unmixing approach, we showed the potential for modeling the fractional water contribution in a mixed LSE spectrum to the corresponding SM content of the sample being measured in the lab. This has implications for estimating SM changes over arid regions using TIR emissivity measurements alone, provided the dry LSE state is known a priori. It should also be noted, however, that since TIR measurements are only sensitive to the top few micrometers of the surface; rapid drying of the surface layer after rainfall events in desert regions would make it difficult to observe these short-term changes from space, which would make correlation with SM content of the top few centimeters of the soil difficult. Nonetheless, we have clearly observed the effect from satellite data.

The AIRS, MOD11B1 v4, and MODTES products showed positive increases in retrieved LSE of between 0.11 and 0.30 (11–30%) at 8.6 μm due to elevated SM after rainfall events over the Namib Desert in Namibia, while no noticeable change was observed for the MOD11B1 v5 LSE product due to a stronger coupling with the Generalized Split-Window (GSW) algorithm which holds the LSE constant in bands 31 and 32. LSE changes were less than 3% for bands 31 and 32. The LSE variations were qualitatively correlated to rainfall estimates from TRMM, and SM estimates from AMSR-E. It was also found that there is a delayed response of 1–2 days between rainfall events and AMSR-E derived SM. Validation of LSE with sand samples collected over the Namib showed that MODTES product most closely matched the lab results with a combined mean absolute difference in all bands of 0.8%, followed by MOD11B1 v4 with 1.0% and v5 with a 1.8% difference.

LST comparisons between MODTES and the standard MODIS products showed that MODTES and MOD11B1 v4 results agreed very well with an R^2 of 0.96 and mean LST bias of -0.8 K. The MOD11B1 v5 and MOD11A1 LSTs were cooler than MODTES with mean differences of 2.1 K and 1.5 K respectively, a result of the LSE being overestimated in these two products.

The continuous monitoring of multiple product versions and algorithms from different data sources is essential for laying down a baseline quality metric to which future climate datasets and trends can be measured. A good example of this is the good agreement in LST between the MODTES and MOD11B1 v4 products which are produced by two independent retrieval algorithms. As a result, a climatology built on either data product can be trusted, whereas if the results of two datasets diverge, then the trends in either are suspect in the absence of rigorous validation.

The ability of retrieval algorithms to observe changes in the LSE after precipitation events is important since the changes can be

significant (8–30% at 8.6 μm , and up to 3% between 11 and 12 μm), which could introduce substantial errors in the land surface temperature and net longwave radiation if not accounted for. To illustrate this, the MODIS broadband emissivity (BBE) results here showed increases of up to 7% in emissivity due to an increase in SM after the Namib rainfall event. Sensitivity studies have shown that this is equivalent to approximately a 5 W/m^2 change in net longwave radiation which is significant when considering the radiative forcing due to greenhouse gases is currently in the 2–3 W/m^2 range. Furthermore, sensitivity studies for split-window algorithms have shown that emissivity errors of only 0.5% in the 11–12 μm window region can result in LST errors of up to 0.7 K. Split-window algorithms using a land classification approach do not account for changes surface SM, and careful consideration should be taken in employing this technique in future missions such as VIIRS (MODIS follow-on).

Acknowledgements

The research described in this paper was carried out at the Jet Propulsion Laboratory, California Institute of Technology, under the contract with the National Aeronautics and Space Administration.

References

- Baldrige, A. M., Hook, S. J., Grove, C. I., & Rivera, G. (2009). The ASTER Spectral Library Version 2.0. *Remote Sensing of Environment*, 114(4), 711–715.
- Berk, A., Anderson, G. P., Acharya, P. K., Bernstein, L. S., Muratov, L., Lee, J., et al. (2005). MODTRAN™ 5, a reformulated atmospheric band model with auxiliary species and practical multiple scattering options: Update. In S. S. Sylvia, & P. E. Lewis (Eds.), *Algorithms and Technologies for Multispectral, Hyperspectral, and Ultraspectral Imagery XI*. Bellingham, WA: Proceedings of SPIE.
- Draper, C. S., Walker, P. J., Steinle, P. J., de Jeu, R. A. M., & Holmes, T. R. H. (2009). An evaluation of AMSR-E derived soil moisture over Australia. *Remote Sensing of Environment*, 113(4), 703–710.
- Fishbein, E., Farmer, C. B., Granger, S. L., Gregorich, D. T., Gunson, M. R., Hannon, S. E., et al. (2003). Formulation and validation of simulated data for the Atmospheric Infrared Sounder (AIRS). *IEEE Transactions on Geoscience and Remote Sensing*, 41(2), 314–329.
- Gillespie, A., Rokugawa, S., Matsunaga, T., Cothren, J. S., Hook, S., & Kahle, A. B. (1998). A temperature and emissivity separation algorithm for Advanced Spaceborne Thermal Emission and Reflection Radiometer (ASTER) images. *IEEE Transactions on Geoscience and Remote Sensing*, 36(4), 1113–1126.
- Hulley, G. C., & Hook, S. J. (2009a). Intercomparison of versions 4, 4.1 and 5 of the MODIS land surface temperature and emissivity products and validation with laboratory measurements of sand samples from the Namib Desert, Namibia. *Remote Sensing of Environment*, 113, 1313–1318. doi:10.1016/j.rse.2009.10.021.1018
- Hulley, G. C., & Hook, S. J. (2009b). The North American ASTER Land Surface Emissivity Database (NAALSED) Version 2.0. *Remote Sensing of Environment*, 113, 1967–1975. doi:10.1016/j.rse.2009.10.051.1005
- Hulley, G. C., Hook, S. J., & Baldrige, A. M. (2009a). Validation of the North American ASTER Land Surface Emissivity Database (NAALSED) Version 2.0 using Pseudo-Invariant Sand Dune Sites. *Remote Sensing of Environment*, 113, 2224–2233.
- Hulley, G. C., Hook, S. J., Manning, E., Lee, S. Y., & Fetzer, E. J. (2009b). Validation of the Atmospheric Infrared Sounder (AIRS) Version 5 (v5) Land Surface Emissivity Product over the Namib and Kalahari Deserts. *Journal of Geophysical Research Atmospheres*, 114, D19104. doi:10.1029/2009JD012351
- Idso, S. B., Reginato, R. J., Jackson, R. D., Kimball, B. A., & Nakayama, F. S. (1974). 3 stages of drying of a field soil. *Soil Science Society of America Journal*, 38(5), 831–837.
- Kealy, P. S., & Hook, S. (1993). Separating temperature & emissivity in thermal infrared multispectral scanner data: Implication for recovering land surface temperatures. *IEEE Transactions on Geoscience and Remote Sensing*, 31(6), 1155–1164.
- Korb, A. R., Salisbury, J. W., & D'Aria, D. M. (1999). Thermal–infrared remote sensing and Kirchhoff's law 2. Field measurements. *Journal of Geophysical Research-Solid Earth*, 104(B7), 15339–15350.
- Lemon, E. R. (1956). The potentialities for decreasing soil moisture evaporation loss. *Soil Science Society of America Journal*, 20, 120–125.
- Lovegrove, B. (1993). *The Living Deserts of Southern Africa*. Vlaeberg: Fernwood Press.
- Matsunaga, T. (1994). A temperature–emissivity separation method using an empirical relationship between the mean, the maximum, & the minimum of the thermal infrared emissivity spectrum. (in Japanese with English abstract). *Journal of Remote Sensing Society of Japan*, 14(2), 230–241.
- Mira, M., Valor, E., Boluda, R., Caselles, V., & Coll, C. (2007). Influence of soil water content on the thermal infrared emissivity of bare soils: Implication for land surface temperature determination. *Journal of Geophysical Research-Earth Surface*, 112(F4), F04003.
- Muller, A., Reason, C. J. C., & Fauchereau, N. (2008). Extreme rainfall in the Namib Desert during late summer 2006 and influences of regional ocean variability. *International Journal of Climatology*, 28(8), 1061–1070.

- Njoku, E. G., & Chan, S. K. (2006). Vegetation and surface roughness effects on AMSR-E land observations. *Remote Sensing of Environment*, 100(2), 190–199.
- Njoku, E. G., Jackson, T. J., Lakshmi, V., Chan, T. K., & Nghiem, S. V. (2003). Soil moisture retrieval from AMSR-E. *IEEE Transactions on Geoscience and Remote Sensing*, 41(2), 215–229.
- Ogawa, K., Schmugge, T., & Rokugawa, S. (2006). Observations of the dependence of the thermal infrared emissivity on soil moisture. *Geophysical Research Abstracts*, 8, 04996.
- Ogawa, K., Schmugge, T., & Rokugawa, S. (2008). Estimating broadband emissivity of arid regions and its seasonal variations using thermal infrared remote sensing. *IEEE Transactions on Geoscience and Remote Sensing*, 46(2), 334–343.
- Oleson, K. W., Bonan, G. B., Levis, S., & Vertenstein, M. (2004). Effects of land use change on North American climate: Impact of surface datasets and model biogeophysics. *Climate Dynamics*, 23(2), 117–132.
- Pellarin, T., Ali, A., Chopin, F., Jobard, I., & Berges, J. C. (2008). Using spaceborne surface soil moisture to constrain satellite precipitation estimates over West Africa. *Geophysical Research Letters*, 35(2).
- Ramsey, M. S., Christensen, P. R., Lancaster, N., & Howard, D. A. (1999). Identification of sand sources and transport pathways at the Kelso Dunes, California, using thermal infrared remote sensing. *Geological Society of America Bulletin*, 111(5), 646–662.
- Salisbury, J. W., & Daria, D. M. (1992). Infrared (8–14 μm) remote-sensing of soil particle-size. *Remote Sensing of Environment*, 42(2), 157–165.
- Salisbury, J. W., Wald, A., & Daria, D. M. (1994). Thermal-infrared remote-sensing and Kirchhoff Law.1. Laboratory measurements. *Journal of Geophysical Research-Solid Earth*, 99(B6), 11897–11911.
- Scheidt, S., Ramsey, M. S., & Lancaster, N. (2010). Determining soil moisture and sediment availability at White Sands Dune Field, NM from apparent thermal inertia (ATI) data. *Journal of Geophysical Research*. doi:10.1029/2009JF001378
- Susskind, J., & Blaisdell, J. (2008). Improved surface parameter retrievals using AIRS/AMSU data. *Proceedings of the SPIE*, 6966. doi:10.1117/1112.774759
- Thomas, D. S. G., Knight, M., & Wiggs, G. F. S. (2005). Remobilization of southern African desert dune systems by twenty-first century global warming. *Nature*, 435(7046), 1218–1221.
- Van Der Kwast, J. (2009). Quantification of top soil moisture patterns; Evaluation of field methods, process-based modelling, remote sensing and an integrated approach.: Knag/Faculteit Geowenschappen Universiteit Utrecht, ISBN 978-90-6809-424-4, Euro 30,00.
- Ventura, F., Snyder, R. L., & Bali, K. M. (2006). Estimating evaporation from bare soil using soil moisture data. *Journal of Irrigation and Drainage Engineering-ASCE*, 132(2), 153–158.
- Wan, Z. M. (2008). New refinements and validation of the MODIS Land-Surface Temperature/Emissivity products. *Remote Sensing of Environment*, 112(1), 59–74.
- Wan, Z. M., & Dozier, J. (1996). A generalized split-window algorithm for retrieving land-surface temperature from space. *IEEE Transactions on Geoscience and Remote Sensing*, 34(4), 892–905.
- Wan, Z. M., & Li, Z. L. (1997). A physics-based algorithm for retrieving land-surface emissivity and temperature from EOS/MODIS data. *IEEE Transactions on Geoscience and Remote Sensing*, 35(4), 980–996.
- Wan, Z. M., Zhang, Y. L., Zhang, Q. C., & Li, Z. L. (2002). Validation of the land-surface temperature products retrieved from Terra Moderate Resolution Imaging Spectroradiometer data. *Remote Sensing of Environment*, 83(1–2), 163–180.
- White, F. (1983). The vegetation of Africa, a descriptive memoir to accompany the UNESCO/AETFAT/UNSO Vegetation Map of Africa (3 Plates, Northwestern Africa, Northeastern Africa, and Southern Africa, 1:5,000,000): UNESCO, Paris.
- Yu, Y. Y., Privette, J. L., & Pinheiro, A. C. (2005). Analysis of the NPOESS VIIRS land surface temperature algorithm using MODIS data. *IEEE Transactions on Geoscience and Remote Sensing*, 43(10), 2340–2350.
- Zhou, L., Dickinson, R. E., Tian, Y., Jin, M., Ogawa, K., Yu, H., et al. (2003). A sensitivity study of climate and energy balance simulations with use of satellite-derived emissivity data over Northern Africa and the Arabian Peninsula. *Journal of Geophysical Research-Atmospheres*, 108(D24), 4795.